Electronic Supplementary Material (ESI) for ChemComm.
This journal is © The Royal Society of Chemistry 2022

Supplementary Information

Confining isolated photosensitizers to relieve self-aggregation and potentiate photodynamic efficacy for synergistic cancer therapy

Gang Liu[a,*], Hui Wang[a], Cai Shi[a], Guanghui Chen[a], Yuqiao Wang[b], Wenjing Huang[c,*], Hao Zhao[b,*]

[a] Pharmacy Department, Renmin Hospital of Wuhan University, Wuhan 430060, China

[b] CAS Key Laboratory for Biomedical Effects of Nanomaterials and Nanosafety, National Center for Nanoscience and Technology of China, Beijing 100190, China

[c] College of Food Science and Engineering, Wuhan Polytechnic University, Wuhan 430023, China

*E-mail: liugang_wh@whu.edu.cn, huangwenjingbest@163.com, zhaoh2021@nanoctr.cn

Contents

1. Supplementary Materials and Methods

Materials. CuCl (Sinopharm Chemical Reagent Co., Ltd., China) was purified with concentrated HCl and water before use [1-3]. Tris(2-dimethyl-aminoethyl)amine (Me_6TREN, purity: >99.0%) was purchased from Alfa Aesar, Shanghai, China. Bis[2-(2'-bromoisobutyryloxy)-ethyl]disulfide (BiBOEDS, purity: >97.0%), poly(ethylene glycol) methyl ether methacrylate (OEGMA, M_n = 300 Da, 1.05 g mL^{-1}) were purchased from Sigma Aldrich, Shanghai, China. 2',7'- Dichlorofluorescin diacetate (DCFH-DA; Cat. No. D6470), 1,3-diphenylisobenzofuran (DPBF; Cat. No. D9130), DNA Content Quantitation Assay (Cell Cycle; Cat. No. CA1510) were purchased from Solarbio Science & Technology Co., Ltd., Beijing, China. 2-(2-methoxyethoxy) ethyl methacrylate (MEO_2MA, purity: >97%, 1.02 g mL^{-1}) was purchased from J&K Scientific Ltd., Beijing, China. Sodium *p*-styrene sulfonate (SS, purity: 90%), *cis*-diammineplatinum dichloride (cisplatin, Pt content >65.0%) was purchased from Macklin Biochemical Co., Ltd., Shanghai, China. meso-Tetra(4-carboxyphenyl) porphine (TCPP, purity: 97%), platinum standard solution (Cat. No. P110723, 1000 ppm Pt, analytical standard, H_2PtCl_6 in 2.0 mol L^{-1} HCl with trace HNO_3) were purchased from Aladdin Reagent Co., Ltd., Beijing, China [4-7]. LysoTracker Green DND-26 (Cat. No. 40738ES50), 4',6-diamidino-2-phenylindole (DAPI; Cat. No. 40727ES10), 3-(4,5-Dimethyl-2-thiazolyl)-2,5-diphenyltetrazolium bromide (MTT; Cat. No. 40201ES72), fetal bovine serum origin South America Gold (FBS; Cat. No. 40130ES76) were purchased from Yeasen Biotechnology Co., Ltd., Shanghai, China. Dihydroethidium (DHE, Cat. No. abs810256) was purchased from Absin Bioscience Inc., China. Deionized water (18.2 MΩ) was used in all experiments. All glassware used in the experiments was cleaned with a 1:1 deionized water/aqua regia solution and rinsed with ultrapure water twice. BALB/c mice (female, 16-18 g) were purchased from the center for disease control and prevention in Hubei Province (Wuhan, China), and housed in the specific-pathogen-free animal facility with controlled humidity (65 ± 5%) and temperature (25 ± 1 °C) under a 12/12-h light/dark cycle with free

access to food and water [8,9]. All animal procedures were approved by the Animal Experimentation Ethics Committee of Wuhan University (license number: SYXK (E) 2020-0027) and performed under the Animal Care and Use Committee guidelines of Renmin Hospital of Wuhan University. The 4T1 subcutaneous tumor model in BALB/c mice was established by inoculation in the right flank (1.2×10^6 4T1 cells per mice). The 4T1-bearing mice were randomly divided into different groups before experiments. At the end of experiments, the 4T1-bearing mice were sacrificed by cervical dislocation according to the AVMA Guidelines for the Euthanasia of Animal: 2020 Edition [10-12].

Synthesis of p(MEO_2MA_{120}-co-$OEGMA_{80}$)-b-pSS_{30} (PES) polymer. Triblock polymer PES was synthesized *via* classical atom transfer radical polymerization (ATRP) [13]. Briefly, MEO_2MA (2.768 mL, 15 mmol), OEGMA (2.857 mL, 10 mmol), BiBOEDS (38 μL, 0.125 mmol), and Me_6TREN (67.5 μL, 0.25 mmol) were mixed with DMSO (5 mL) in a sealed Schlenk tube. After four cycles of sequential liquid nitrogen frozen (5 min), vacuum (8 min), and argon-filling under vigorous stirring in 60 °C water bath (10 min), purified CuCl (25 mg, 0.25 mmol) was added into the above system to initialize polymerization. Reacting at 60 °C for 24 h, *p*(MEO_2MA_{120}-*co*-$OEGMA_{80}$) (PE), the first block polymer, was obtained. Afterward, degassed sodium *p*-styrenesulfonate (SS, 0.86g, 3.75 mmol) DMSO solution (4 mL) was injected into the reaction system and reacted for another 72 h at 110 °C. The purified PES was acquired by dialysis and stored in a vacuum desiccator for further use. The composition and molecular weight of these polymers were verified using a nuclear magnetic resonance spectrometer (600 MHz, AV400, Bruker, Switzerland) and Malvern Viscotek gel permeation chromatography (GPC) with 0.01 M sodium nitrate solution (pH 7.0) as mobile phase.

Constructing cisplatin coordinated nanoscale coordination polymers (NCPs) with TCPP and PES (Pt/TCPP NCPs). First, cisplatin was converted into diaquated (NO_3^-/aquo/hydroxo) species by mixing with $AgNO_3$ at the molar ratio of 2:1, replacing chloride ions with more

labile ligands—nitrate (NO_3^-), aquo, and hydroxo groups [14]. To elaborate, cisplatin (10 mg) was suspended in 20 mL distilled water and mixed with $AgNO_3$ ([$AgNO_3$]/[cisplatin] = 2) to form the aqueous complex. The solution was stirred in the dark at room temperature for 12 h. A white precipitate of AgCl was observed, indicating the proceeding of the reaction. The mixture was then centrifuged at 8000 rpm for 20 min to remove most of the AgCl precipitate; to completely remove the AgCl precipitate, the supernatant was purified by passing through a 0.22 μm filter [15]. Then, diaquated (NO_3^-/aquo/hydroxo) species was further used for coordination with a deprotonated carboxylic group (-COO^-) of TCPP and sulfonate ligand (-SO_3^-) of PES to construct Pt/TCPP NCPs. Briefly, taking the PES/TCPP ratio of 12 as an example (PES/TCPP ratio indicated the molar ratio of the -SO_3^- in PES and the -COO^- in TCPP), 10 mL TCPP (0.759 mM of TCPP including 3.035 mM of -COO^-) DMSO solution was mixed with 10 mL PES (1.208 mM of PES including 36.226 mM of -SO_3^-) aqueous solution in a 100 mL flask at 25 °C under gentle stirring. After 3 min, 20 mL of deionized water was added into the above mixture to obtain a clear solution. Afterward, 10 mL diaquated (NO_3^-/aquo/hydroxo) species (19.563 mM) aqueous solution was injected into the mixed solution at a speed of 20 mL h^{-1} using a micro-infusion pump (LD-P2020II, Shanghai Lande Medical Instrument Co., Ltd., Shanghai, China). Stirring gently for another 24 h at 25 °C, the resultant Pt/TCPP NCPs were purified by ultrafiltration (6,000 rpm × 10 min, MWCO: 100 kDa). Similarly, nontoxic Mg^{2+} ions coordinated with TCPP and PES to form TCPP NCPs as single photodynamic therapy control, while diaquated (NO_3^-/aquo/hydroxo) species coordinated with PES to form Pt NCPs as single chemotherapy control.

Characterization. The hydrodynamic diameter of Pt/TCPP NCPs was determined by dynamic light scattering (Zetasizer Nano ZS90, Malvern Instruments Co., Ltd., Malvern, UK). The morphology of Pt/TCPP NCPs was observed by using a transmission electron microscope (TEM, Tecnai G2 20, FEI Corp., Netherlands). Fluorescence emission spectra of Pt/TCPP NCPs were acquired from a fluorescence spectrophotometer (Hitachi F-4500).

Drug loading and release property of Pt/TCPP NCPs. The TCPP-loading capacity of Pt/TCPP NCPs at the PES/TCPP ratio of 12 was measured by a subtraction method [16]. Briefly, after ultrafiltration purification, the ultrafiltrate from Pt/TCPP NCPs was collected. A fluorescence spectrophotometer was used to measure the concentration of unloaded TCPP. The parameters of the instrument were excitation wavelength (515 nm), and emission wavelength (653nm). Therefore, the amount of TCPP loaded in Pt/TCPP NCPs was calculated by subtracting the unloaded amount of TCPP from the total feed of TCPP. The cisplatin-loading capacity of Pt/TCPP NCPs was measured by direct measurement. In brief, 50 μL of refined Pt/TCPP NCPs was digested using concentrated nitric acid (65–68%) and perchloric acid (70–72%) at the volume ratio of 4:1 at 320 °C. After 0.5 h, the digested solutions got clear and diluted to 10 mL with deionized water for measuring Pt concentration using microwave plasma atomic emission spectrometer (MP-AES, Agilent 4100, Agilent Technologies, Santa Clara, California, USA) [6]. The encapsulation efficiency (EE) was calculated according to Eq. (S1).

$$EE = \frac{C_f \cdot V_f}{W_0} \times 100\% \quad \text{(S1)}$$

Here, W_0 is the feeding amount of TCPP or cisplatin, and C_f and V_f are the concentration and volume of TCPP or cisplatin contained in Pt/TCPP NCPs dispersions, respectively.

In vitro release behavior of cisplatin from Pt/TCPP NCPs at the PES/TCPP ratio of 12 was studied using a dialysis method against 50 mL of PBS buffer (6.7 mmol L^{-1}) at pH 5.0 and 7.4 (release media) at 37 °C [16]. In brief, 1 mL Pt/TCPP NCPs dispersion was added into a dialysis bag (MWCO: 3500 Da) and put into release media with constant shaking at 120 rpm min^{-1} at 37 °C. At 3, 6, 9, 18, and 36 h, 50 mL of release media was taken out and replenished with an equal volume of fresh media. The released media was taken to determine the released cisplatin amount using MP-AES. The whole releasing process was shielded from light. The accumulative release (AR, %) of cisplatin was calculated following Eq. (S2).

$$AR = \frac{\sum_{i=1}^{m} C_i V_i}{C_0 V_0} \times 100\% \quad \text{(S2)}$$

Here, C_i and V_i are the concentration and volume of cisplatin from the sample of No. i, respectively. C_0 is the total cisplatin concentration in Pt/TCPP NCPs dispersions, and V_0 is the volume of Pt/TCPP NCPs dispersions.

Singlet oxygen ($^1O_2$) generation of Pt/TCPP NCPs under 660 nm laser irradiation. The $^1O_2$ generation ability of Pt/TCPP NCPs under 660 nm laser (MRL-III-FS-660-800 mW, Changchun New Industries Optoelectronics Tech. Co., Ltd, China) irradiation was measured using 1,3-Diphenylbenzofuran (DPBF) as a probe. In brief, the aqueous solution of Pt/TCPP NCPs at different PES/TCPP ratios (4 μg mL^{-1} of TCPP, 2 mL) was mixed with DPBF (500 μg mL^{-1}, 150 μL) in a quartz cuvette. Then, the mixed solution was irradiated with a 660 nm laser (100 mW cm^{-2}), and the absorbances of DPBF at 415 nm were recorded every 30 s. For the singlet oxygen quantum yield (Φ_Δ) investigation of Pt-ICG/PES, free TCPP was selected as a reference (Φ_Δ^{TCPP} = 0.58 in water) [17]. Φ_Δ was calculated using Eq. (S3) [18].

$$\Phi_\Delta = \Phi_\Delta^{TCPP} \times \frac{k_{Pt/TCPP\ NCPs} \cdot F_{TCPP}}{k_{TCPP} \cdot F_{Pt/TCPP\ NCPs}} \quad \text{(S3)}$$

Where k is the slope of the absorbance of DPBF at 415 nm versus irradiation time, and F is the absorption correction factor calculated by $F = 1 - 10^{OD}$ (OD is the optical density at the irradiation wavelength).

Cellular uptake, intracellular $^1O_2$ generation, and lysosomal disruption. 4T1 cells (4×10^6) were seeded in a Petri dish (Φ = 15 cm) at 37 °C. After being cultured for 12 h, the media were replaced by Pt/TCPP NCPs at the PES/TCPP ratio of 12 containing fresh media (0.23 μg mL^{-1} TCPP, 2.2 μg mL^{-1} cisplatin) and cultured for another 4 h. Then, 4T1 cells were washed with cold PBS 3 times, incubated with 2 mL of trypsin for 5 min at 37 °C, and enumerated after centrifuge collection, followed by liquid nitrogen flash freezing (5 min) and sonication (15

min). The above steps were repeated three times. Then, TCPP from the cells was extracted using the complex solution of H_2O/DMSO/HCl (volume ratio was 30/55/15, HCl concentration was 37%) at the volume ratio of 3/1. After 30 min-vortex and 10-min centrifugation (10,000 rpm), the supernatant was obtained, and the TCPP concentration was measured using a fluorescence spectrophotometer [19]. The intracellular cisplatin amounts were detected using a microwave plasma atomic emission spectrometer (MP-AES, Agilent 4100, Agilent Technologies, Santa Clara, California, USA) following digestion with the mixed nitric acid-perchloric acid solution [20].

The intracellular $^1O_2$ generation of Pt/TCPP NCPs at the PES/TCPP ratio of 12 under irradiation was investigated using flow cytometry, probed by 2'-7' dichlorofluorescein diacetate (DCFH-DA) [21]. 4T1 cells (5×10^5 per well) were seeded in a 6-well plate at 37 ^oC. After being cultured for 12 h, the media were replaced by Pt/TCPP NCPs at the PES/TCPP ratio of 12 containing fresh media (0.12 μg mL^{-1} TCPP, 1.1 μg mL^{-1} cisplatin) and cultured for another 4 h. Then, Pt/TCPP NCPs containing media were removed, and 4T1 cells were washed with cold PBS 3 times and incubated with DCFH-DA solution (10 μmol L^{-1}) for 30 min. Afterward, DCFH-DA solution was removed, and 4T1 cells were washed with cold PBS 3 times and incubated with 2 mL of trypsin for 5 min at 37 ^oC. 4T1 cells were then collected in flow tubes. Immediately, cells were irradiated with a 660 nm laser (100 mW cm^{-2}) for 8 min (light dose: 48 J cm^{-2}, lower than the clinically recommended light dose 50 J cm^{-2}) [22] and collected for flow cytometric analysis.

The lysosomal disruption ability of Pt/TCPP NCPs under 660 nm laser irradiation was studied by staining 4T1 cells with Lysotracker Green DND-26 and DAPI [23]. 4T1 cells were seeded in confocal dishes at a density of 3×10^5 cells per dish overnight and then incubated with Pt/TCPP NCPs (0.12 μg mL^{-1} TCPP, 1.1 μg mL^{-1} cisplatin) for 1 h. Subsequently, 4T1 cells were irradiated with 660 nm light (100 mW cm^{-2}) for 8 min (light dose: 48 J cm^{-2}) after replacing cell media with fresh cell media. Afterward, Lysotraker Green DND-26 (0.5 mL, 100

nmol L^{-1}) was added for labeling lysosome at 37 °C for 45 min. Subsequently, 4T1 cells were fixed with 4% paraformaldehyde for 20 min after being washed with cold PBS 3 times. Finally, 4T1 cells were stained with DAPI (5.0 μg mL^{-1}, 100 μL each dish) for 20 min and then observed using a confocal light scanning microscopy (CLSM, Olympus IX81, Japan) to obtain fluorescence images.

Cytotoxicity of Pt/TCPP NCPs on 4T1 and cisplatin-resistant A549/Pt cells. The cytotoxicity of Pt/TCPP NCPs on 4T1 and cisplatin-resistant A549/Pt cells was investigated by MTT assay [16]. Briefly, 4T1 or A549/Pt cells were incubated in 96-well plates at a cell density of 1.0×10^4 for each well. After 12 h, the media were replaced with various materials at different concentrations and the cells were cultured for another 4 h (4T1) or 12 h (A549/Pt). Afterward, the media containing different materials were removed, and the cells were washed with cold PBS twice. Then, 4T1 or A549/Pt cells were irradiated with a 660 nm laser (100 mW cm^{-2}) for 8 min (light dose: 48 J cm^{-2}) or not. After being cultured for another 20 h (4T1) or 12 h (A549/Pt), 200 μL of MTT containing 20 μL of mother liquor (5 mg mL^{-1}) and 180 μL of RPMI 1640 media was added in every well, and the optical densities (ODs) at 492 nm were measured 15 min later. The blank and negative controls were serum-free RPMI 1640 media and the mixture solution of serum-free RPMI 1640 media and 4T1 or A549/Pt cells, respectively. Then, the cell viability (CV) was calculated following Eq. (S4):

$$CV = \frac{OD_s - OD_b}{OD_n - OD_b} \times 100\% \quad \text{(S4)}$$

Here, OD_s, OD_b, and OD_n were the OD values of samples, blank control, and negative control, respectively.

The cooperative index (CI) of Pt/TCPP NCPs was calculated following Eq. (S5) [6]:

$$CI = \frac{D_{\text{Pt/TCPP NCPs + laser}^{TCPP}}}{(D_0)_{\text{TCPP NCPs + laser}^{TCPP}}} + \frac{D_{\text{Pt/TCPP NCPs + laser}^{Cisplatin}}}{(D_0)_{\text{Pt NCPs + laser}^{Cisplatin}}} \quad \text{(S5)}$$

Here, $(D_0)_{\text{TCPP NCPs + laser}^{TCPP}}$ and $(D_0)_{\text{Pt NCPs + laser}^{Cisplatin}}$ represented the half-maximal inhibitory

concentration (IC_{50}) value of TCPP in TCPP NCPs and cisplatin in Pt NCPs under 660 nm laser irradiation, respectively. $D_{Pt/TCPP\ NCPs\ +\ laser}^{TCPP}$ and $D_{Pt/TCPP\ NCPs\ +\ laser}^{Cisplatin}$ represented the corresponding IC_{50} of TCPP and cisplatin in Pt/TCPP NCPs under 660 nm laser irradiation.

Cell-cycle detection. Briefly, 4T1 cells were incubated in 96-well plates at a cell density of 1.0×10^4 for each well. After 12 h, the media were replaced with various materials at different concentrations and the cells were cultured for another 4 h. Afterwards, the media containing different materials were removed and the cells were washed with cold PBS twice. Then, 4T1 cells were irradiated with a 660 nm laser (100 mW cm^{-2}) for 8 min (light dose: 48 J cm^{-2}) or not and then allowed to incubate for another 12 h in the dark. After treatment, cells were lysed with 70% ethanol (diluted with PBS, 4 °C, 2 h), incubated with RNaseA (100 μg mL^{-1}, 37 °C, 30 min), and stained with PI (100 μg mL^{-1}, 4 °C, 30 min) and analyzed *via* flow cytometry (NovoCyte, Agilent).

In vivo behavior of Pt/TCPP NCPs. The intratumoral retention ability of Pt/TCPP NCPs was evaluated on 4T1-bearing BALB/c mice. Pt/TCPP NCPs at the PES/TCPP ratio of 12 or Pt+TCPP solutions were *i.t.* injected into tumors at a dose of 0.10 mg kg^{-1} TCPP, 0.96 mg kg^{-1} cisplatin. At 0.5 h, 2 h, 4 h, and 8 h post-injection, the tumors were harvested and ground by a homogenizer. The TCPP was extracted using the complex solution of H_2O/DMSO/HCl (volume ratio was 30/55/15, HCl was concentrated hydochloric acid, 37% by volume) at the volume ratio of 3/1; the concentration was measured by a fluorescence spectrophotometer. The intratumoral cisplatin amounts were detected using MP-AES, following digestion with the mixed nitric acid-perchloric acid solution.

Ex vivo ROS evaluation. The intratumoral ROS generation level was detected by dihydroethidium (DHE) staining [18]. Briefly, 20.0 μmol kg^{-1} DHE was *i.t.* injected into tumors. After 0.5 h, Pt/TCPP NCPs (0.10 mg kg^{-1} TCPP, 0.96 mg kg^{-1} cisplatin) were *i.t.* injected into tumors. Then, the tumors were irradiated with a 660 nm laser (100 mW cm^{-2}) for 8 min (light

dose: 48 J cm^{-2}). Subsequently, the tumors were resected and sectioned for observation using CLSM.

Antitumor efficacy evaluation of Pt/TCPP NCPs. The 4T1 tumor-bearing BALB/c mice model was established to investigate the antitumor efficacy of different materials [23]. BALB/c mice were subcutaneously inoculated with 4T1 cells (1.2×10^6 cells per mouse) in the right flank. The mice were randomly divided into nine groups, including G1: PBS buffer, G2: free cisplatin plus free TCPP (Pt+TCPP), G3: Pt+TCPP + laser, G4: Pt NCPs, G5: Pt NCPs + laser, G6: TCPP NCPs, G7: TCPP NCPs + laser, G8: Pt/TCPP NCPs, G9: Pt/TCPP NCPs + laser. The mice were *i.t.* injected with different materials at the dose of 0.10 mg kg^{-1} TCPP, and 0.96 mg kg^{-1} cisplatin. The tumor volume (V) was measured every day with a vernier caliper according to Eq. (S6):

$$V = \frac{L \times W^2}{2} \quad \text{(S6)}$$

Here, L and W were the length and width values (mm) of tumors, respectively.

At the end of the experiment, the mice were euthanized, and their major tissues and tumors were harvested for histologic analysis and immunohistochemical analysis. Lung tissues were fixed with Bouin's fixer for 0.5 h before counting pulmonary metastatic nodules.

Serum biochemistry assessment. Pt/TCPP NCPs (0.10 mg kg^{-1} TCPP, 0.96 mg kg^{-1} cisplatin) were *i.t.* injected into 4T1-bearing BALB/c mice (female). The mice were euthanized at 1, 10, and 20 days post-injection, and their blood was collected for serum biochemistry and hematological assessments. Untreated mice were selected as the control [6].

Statistical analysis. Quantitative data are expressed as mean ± standard deviation (SD) from sample numbers (n). For statistical significance, unpaired Student's *t*-test was used to compare two groups; for multiple groups, one-way ANOVA was used. $*P < 0.05$; $**P < 0.01$; $***P < 0.001$.

2. Supplementary Scheme and Figures

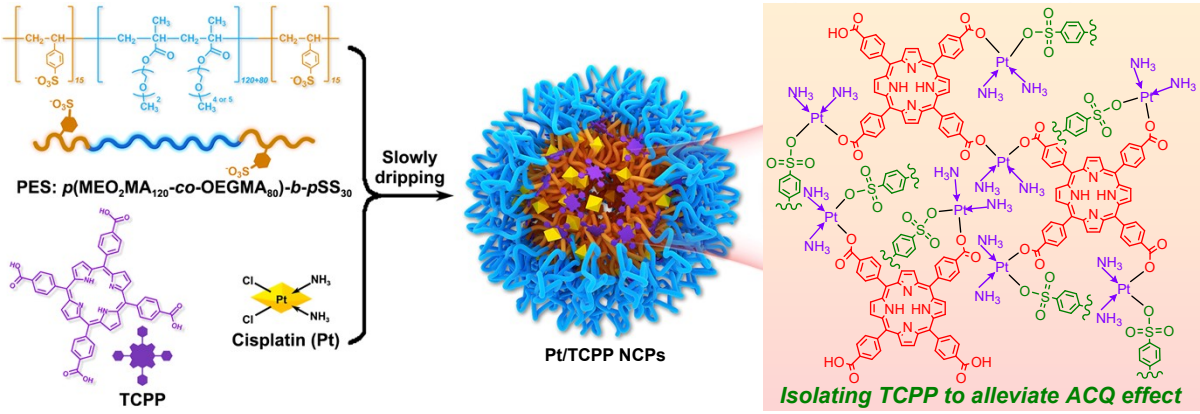

Scheme S1. Schematic illustration of fabrication of Pt/TCPP NCPs.

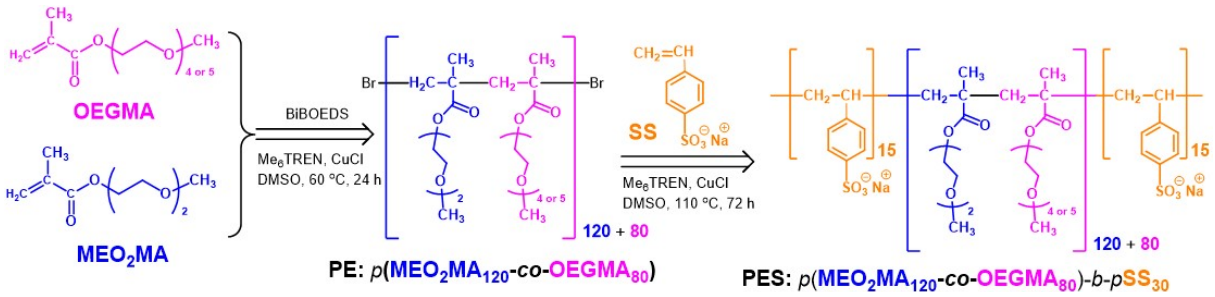

Fig. S1. The synthetic routes of $p(MEO_2MA_{120}$-*co*-$OEGMA_{80})$ (PE) and $p(MEO_2MA_{120}$-*co*-$OEGMA_{80})$-*b*-pSS_{30} (PES) polymers *via* atom transfer radical polymerization (ATRP).

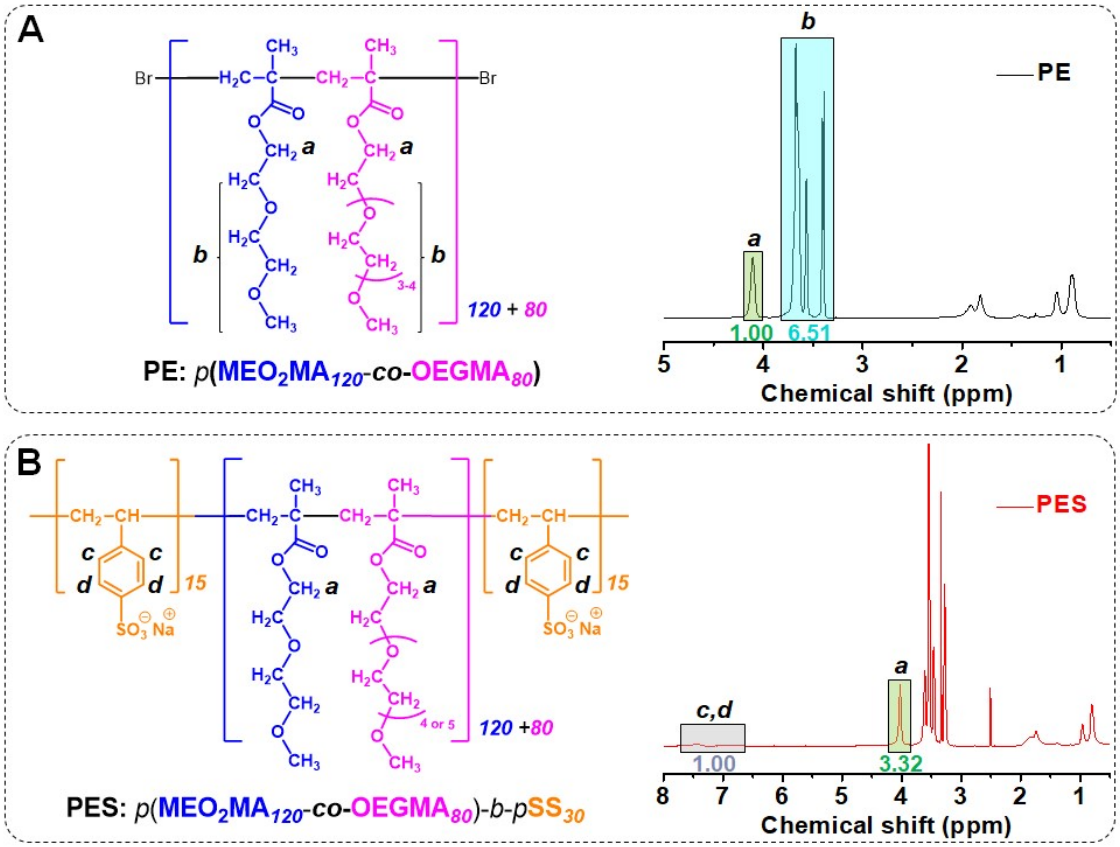

Fig. S2. (A) Molecular structure and ^{1}H-NMR characterization of PE ($CDCl_3$, 600M Hz). (B) Molecular structure and ^{1}H-NMR characterization of PES (DMSO-d_6, 600M Hz).

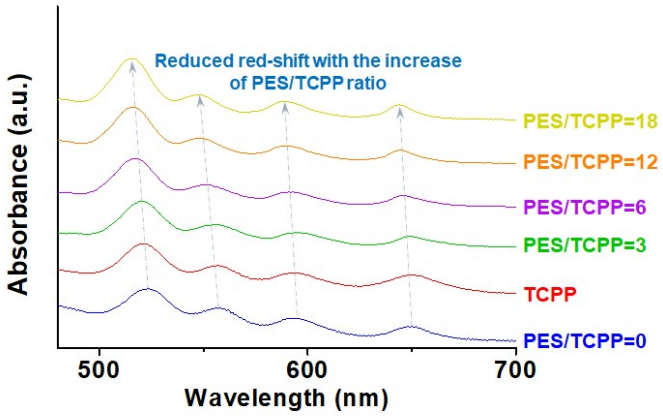

Fig. S3. Vis-NIR absorption spectra of Pt/TCPP NCPs at different PES/TCPP ratios and free TCPP aqueous solution (10 μg mL^{-1} of TCPP).

In an aqueous solution, TCPP molecules tend to form *J*-aggregates (causing red-shift of absorption spectra) and *H*-aggregates (causing blue-shift of absorption spectra) driven by π–π stacking [24], and *J*-aggregates dominate from the Vis-NIR absorption spectra [25,26]. As the PES/TCPP ratio increased from 0 to 18, the absorption spectra red-shift degree of Pt/TCPP NCPs weakened gradually, indicating the PES acts as an isolator that prevents the formation of *J*-aggregates of TCPP, mitigating the ACQ effect.

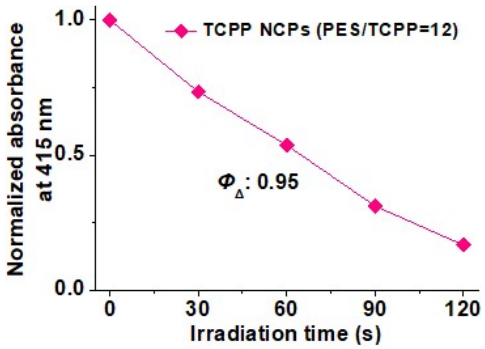

Fig. S4. Normalized absorbance of ROS probe DPBF at 415 nm in the presence of TCPP/PES NCPs at the PES/TCPP ratio of 12 under 660 nm laser irradiation. PES/TCPP ratio indicated the molar ratio of the sulfonates in PES and the carboxylic groups in TCPP.

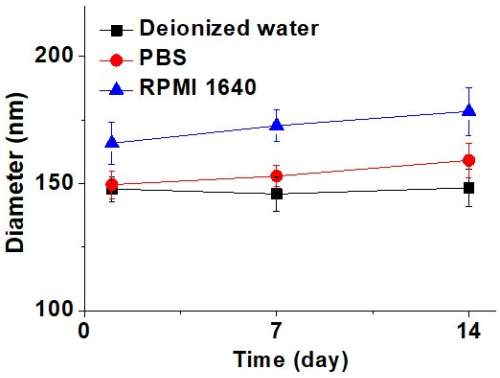

Fig. S5. Hydrodynamic diameters of Pt/TCPP NCPs at the PES/TCPP ratio of 12 dispersed in different media and stored for varying times.

After being dispersed in different media (including deionized water, PBS, and RPMI 1640) for two weeks, the hydrodynamic diameters of Pt/TCPP NCPs remained stable, suggesting that Pt/TCPP NCPs had satisfying colloidal stability.

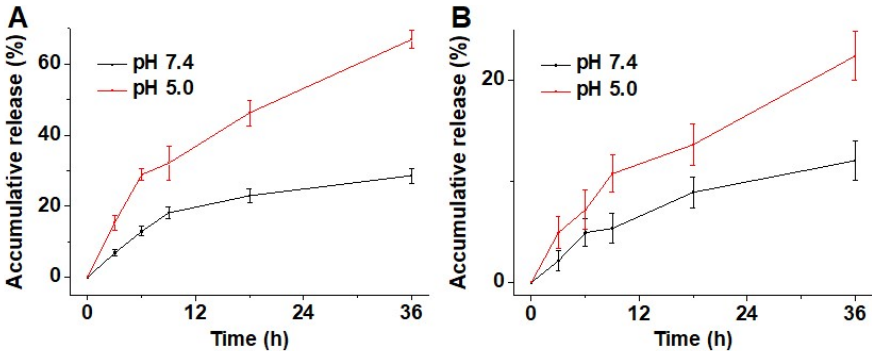

Fig. S6. (A) Accumulative release profiles of cisplatin from Pt NCPs under pH 5.0 and 7.4. (B) Accumulative release profiles of TCPP from Pt NCPs at the PES/TCPP ratio of 12 under pH 5.0 and 7.4.

As shown in Fig. 1F and S6A, Pt/TCPP NCPs and Pt NCPs exhibited similar cisplatin release behavior, indicating Pt NCPs could be used as a control for single chemotherapy.

As shown in Fig. 1F and S6B, it could be found that the accumulative release amount of TCPP is significantly lower than that of Pt under the same release conditions. A likely reason is that compared to the size of TCPP, the smaller Pt is easier to diffuse from the three-dimensional network of Pt/TCPP NCPs [27]. Indeed, the released photosensitizers can come into contact with more oxygen molecules and thus undergo energy transfer under the excitation of light, generating more singlet oxygen. However, recent studies have shown that photosensitizers loaded in nanoparticles can also react with oxygen diffusing into nanoparticles to form singlet oxygen without being released [28-30]. In fact, TCPPs are still prone to self-aggregation after release from NCPs, leading to a compromised PDT performance. In contrast, the Pt/TCPP NCPs prepared in this work confine TCPP in NCPs and prevent self-aggregation of TCPP molecules by the steric hindrance effect of the PES isolator, thus maintaining the excellent PDT performance of TCPP molecules (Scheme 1A). And such a selective release behavior of TCPP is highly desirable for PES to prevent self-aggregation of TCPP molecules, thus maintaining their durable PDT performance and ultimately facilitating synergistic cancer PDT/chemotherapy.

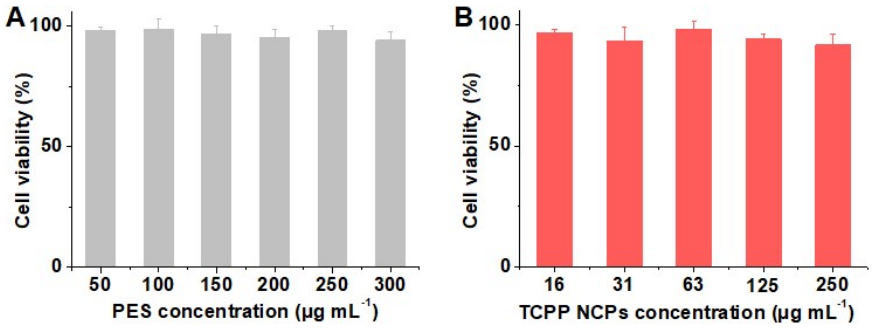

Fig. S7. Cell viability curves of NIH3T3 cells after 24 h incubation with (A) PES and (B) TCPP NCPs at different concentrations without 660 nm laser irradiation.

Before evaluating the phototoxicity of cancer cells, the biocompatibility of this nano-formulation was investigated on NIH3T3 mouse fibroblasts *in vitro*. Since Pt/TCPP NCPs mainly comprise PES, and the toxicity of cisplatin distorts the biocompatibility of this nano-formulation, we constructed TCPP NCPs with non-toxic Mg^{2+} ions. Therefore, we verified the biocompatibility of PES and TCPP NCPs on NIH3T3 mouse fibroblasts, by evaluating their cytotoxicity. After incubation with PES and TCPP NCPs for 24 h, the cell viability of NIH3T3 cells remained 90% even at PES concentration of 300 μg mL^{-1} and at TCPP NCPs NCPs concentration of 250 μg mL^{-1}, indicating the good biosafety of this nano-formulation.

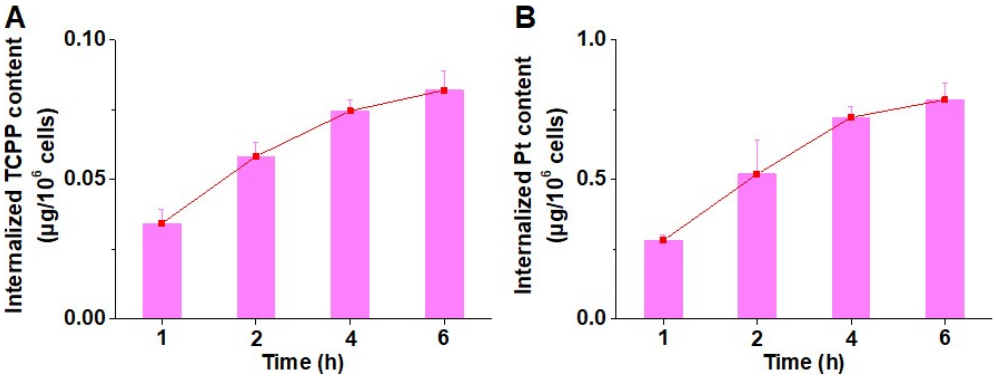

Fig. S8. Cellular uptake amounts of (A) TCPP and (B) cisplatin by 4T1 cells after incubation with Pt/TCPP NCPs (0.23 μg mL^{-1} TCPP, 2.2 μg mL^{-1} cisplatin) for different times.

During the first 4 h, the cellular uptake amounts of Pt/TCPP NCPs by 4T1 cells continued to increase. After 4 h of incubation, however, the increase in the uptake amount of Pt/TCPP NCPs by 4T1 cells became insignificant. Therefore, we co-incubated the Pt/TCPP NCPs with 4T1 cells for 4 h for subsequent experiments.

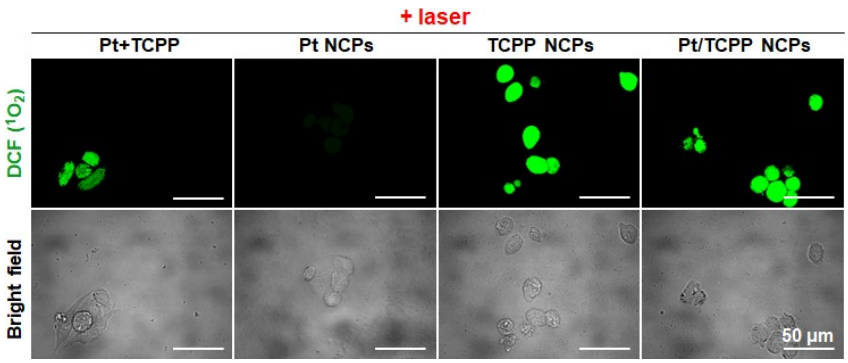

Fig. S9. Fluorescence images of 4T1 cells stained by DCFH-DA under 660 nm laser (100 mW cm^{-2}) irradiation for 8 min after incubation with Pt+TCPP, Pt NCPs, TCPP NCPs, and Pt/TCPP NCPs (0.12 μg mL^{-1} TCPP, 1.1 μg mL^{-1} cisplatin) for 4 h.

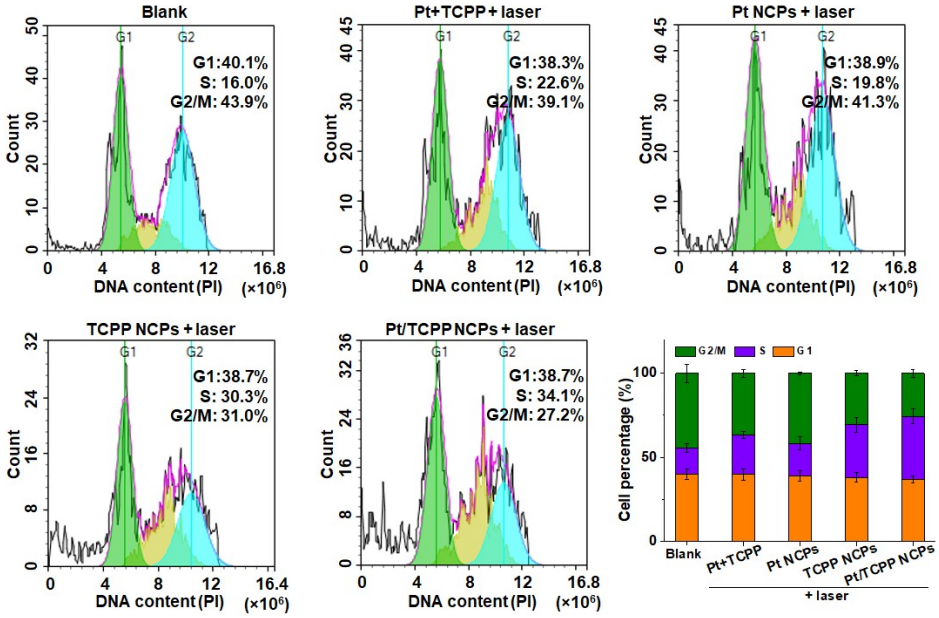

Fig. S10. Cell cycle analysis of 4T1 cells by flow cytometry after incubation with Pt+TCPP, Pt NCPs, TCPP NCPs, and Pt/TCPP NCPs (0.12 μg mL^{-1} TCPP, 1.1 μg mL^{-1} cisplatin) under 660 nm laser irradiation for 8 min. "Blank group" indicated the 4T1 cells without any treatment.

We evaluated the effects of Pt/TCPP NCPs under laser irradiation on the cell cycle of 4T1 cancer cells. According to the FACS plots, the S-phase increased from 16.0% (Blank group) to 19.8% and 30.3% in these cancer cells after being treated with Pt NCPs and TCPP NCPs under 660 nm laser irradiation, indicating a delay in the cell cycle was caused by cisplatin and intracellular ROS amplification. Moreover, the S-phase further increased to 34.1% in the 4T1 cells treated with Pt/TCPP NCPs under irradiation, which suggested that the synergistic PDT/chemotherapy of Pt/TCPP NCPs induced significant cell-cycle arrest.

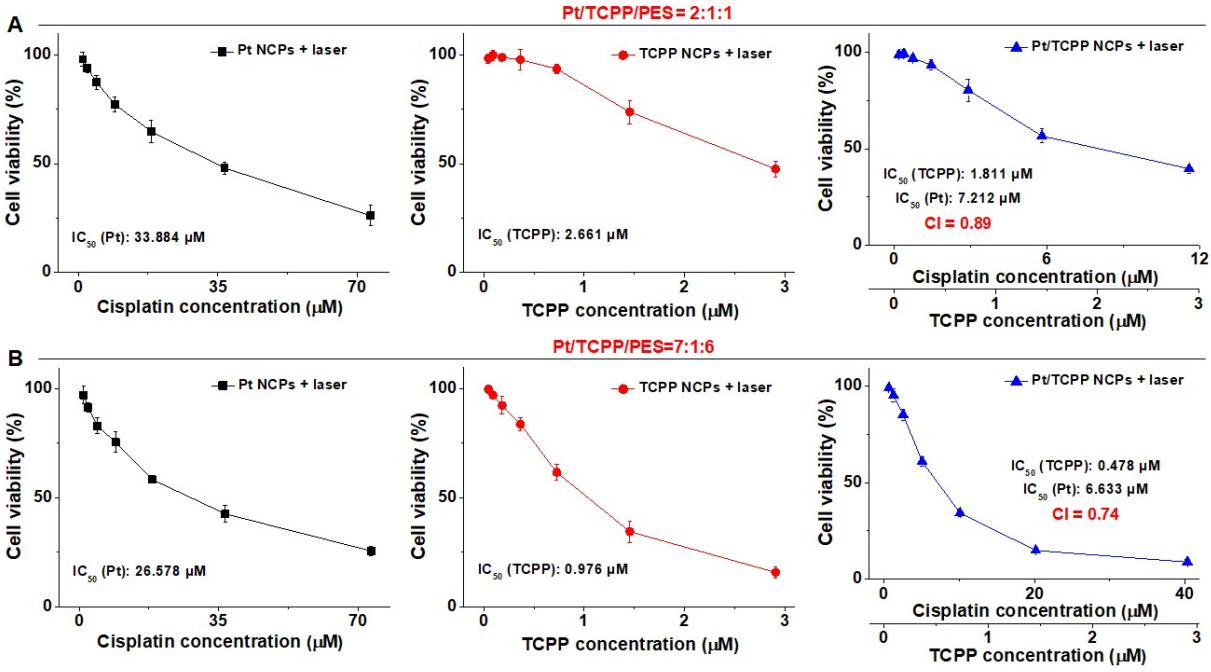

Fig. S11. Cell viability curves of 4T1 cells with 660 nm laser irradiation after incubation with Pt/TCPP NCPs at various PES/TCPP ratios.

We selected Pt/TCPP NCP (Pt/TCPP/PES=13:1:12) (robust PDT effect), Pt/TCPP NCP (Pt/TCPP/PES=7:1:6) (modest PDT effect), and Pt/TCPP NCP (Pt/TCPP/PES=2:1:1) (poor PDT effect) to study the influence of Pt/TCPP ratio on the synergistic effect of the chemotherapy/PDT. As shown in Fig. S11, it could be found that the cooperative index (CI) for PDT/chemotherapy of Pt/TCPP NCPs was highly related to the degree of aggregation alleviation (reflected by the PES/TCPP ratio). CI values decreased from 0.89, 0.74 to 0.63 as the PES/TCPP ratios increase from 1, 6 to 12, suggesting we can regulate the synergistic effect of PDT/chemotherapy by tailoring PES/TCPP ratios, which is beneficial to increase antitumor efficacy and reduce side-effects.

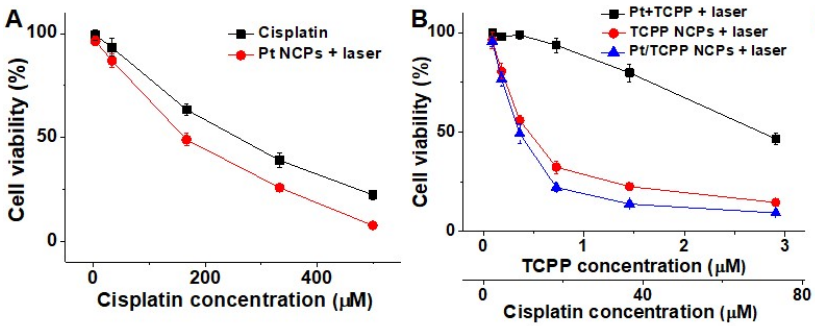

C

	IC_{50} (μM)	
	TCPP	Cisplatin
Cisplatin	/	247.87
Pt+TCPP + laser	2.74	69.14
Pt NCPs + laser	/	167.76
TCPP NCPs +laser	0.43	/
Pt/TCPP NCPs +laser	0.35	8.75

Fig. S12. Cell viability curves of cisplatin-resistant A549 cells (A549/Pt) with 660 nm laser irradiation after incubation with Pt/TCPP NCPs and other materials.

As A549/Pt cells showed obvious resistance effect on cisplatin (Fig. S12A), the resistance could somehow be overcome by loading cisplatin into Pt NCPs. Moreover, owing to the enhanced synergistic PDT/chemotherapy, the proliferation of A549/Pt cells was depressed by Pt/TCPP NCPs under 660 nm laser irradiation, with CI value of 0.87 (Fig. S12B, C). These results indicated that Pt/TCPP NCPs not only kill cisplatin-sensitive 4T1 cells efficiently, but also reverse the resistance of A549/Pt cells and inhibit their growth effectively.

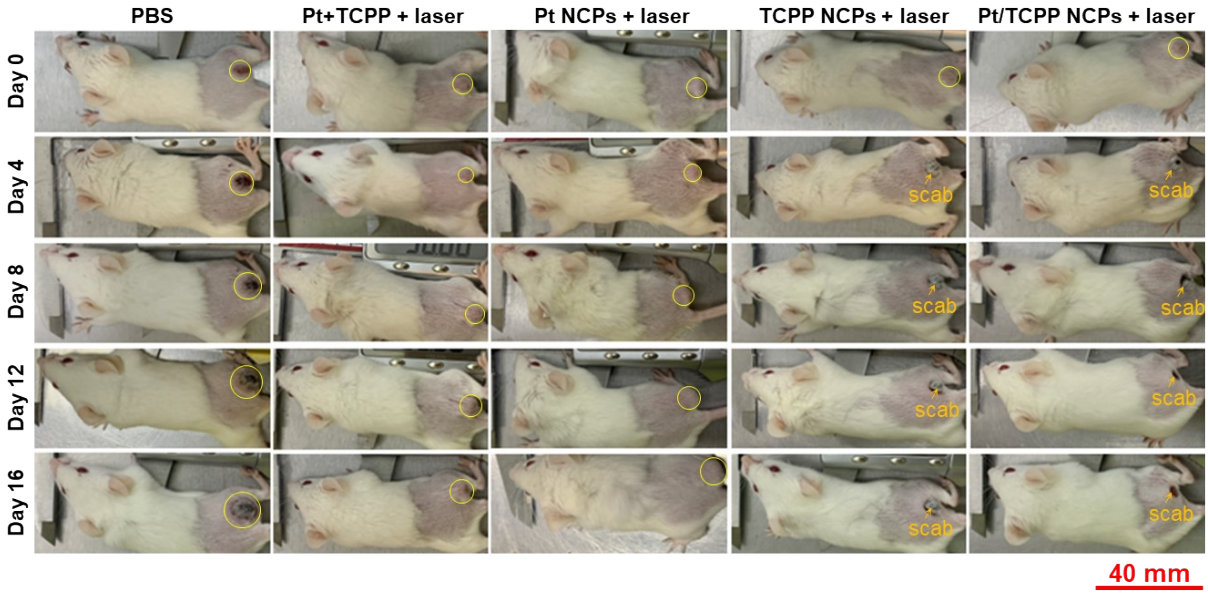

Fig. S13. Representative mice photographs at days 0, 4, 8, 12, 16, and 20 after various treatments including PBS, Pt+TCPP + laser, Pt NCPs + laser, TCPP NCPs + laser, and Pt/TCPP NCPs + laser. The areas indicated by the yellow circles represent tumors.

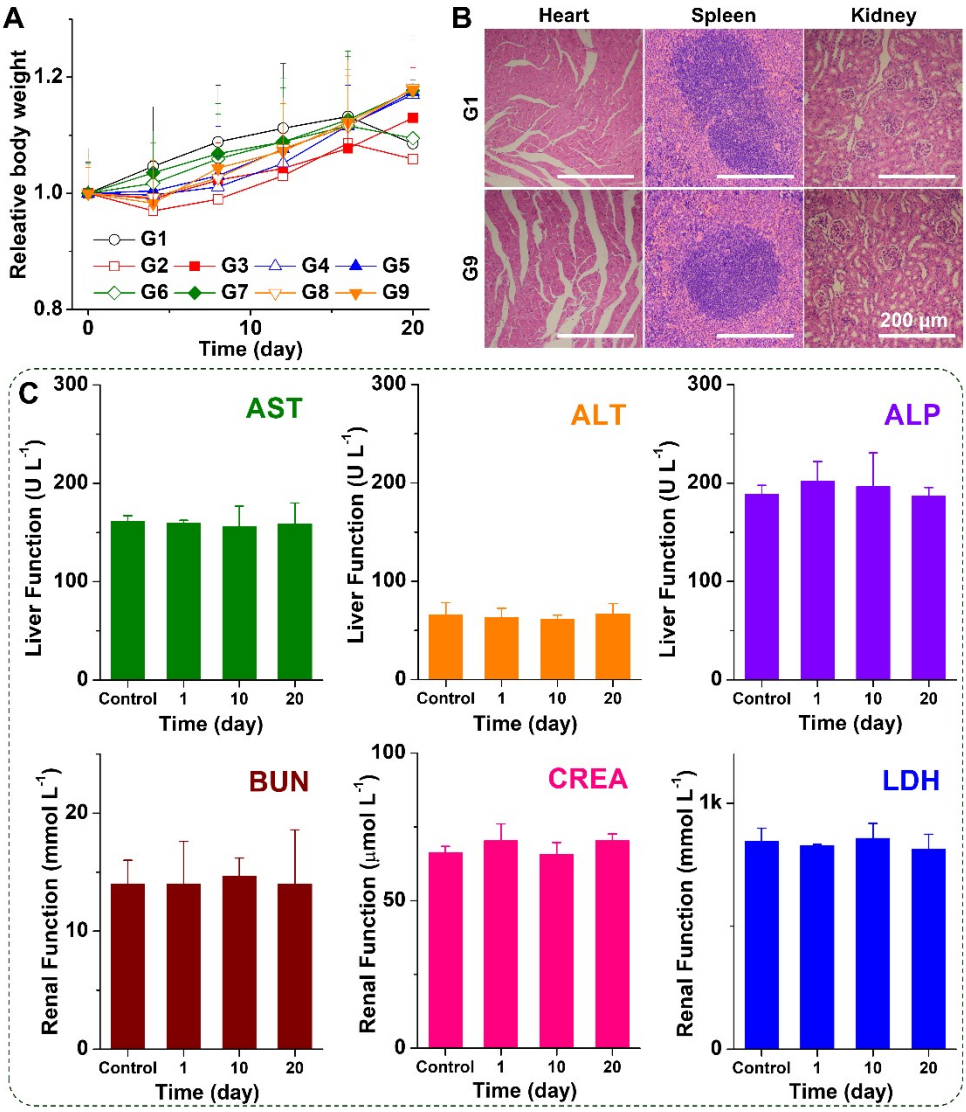

Fig. S14. Biocompatibility of Pt/TCPP NCPs at the PES/TCPP ratio of 12 in 4T1 tumor-bearing BALB/c mice. (A) Bodyweight curves of 4T1tumor-bearing BALB/c mice during 20 days of different treatments (0.10 mg kg^{-1} TCPP, 0.96 mg kg^{-1} cisplatin, *i.t.* injection). Data are mean ± SD, n = 5. (B) H&E staining of the hearts, spleens and kidneys from the mice 20 days post-treatment. (C) Serum biochemistry assessment, including three indicators of liver function (AST, ALT and ALP) and three indicators of renal function (BUN, CREA and LDH), on the 4T1 tumor-bearing BALB/c mice at different times post-treatment with Pt/TCPP NCPs (0.10 mg kg^{-1} TCPP, 0.96 mg kg^{-1} cisplatin, *i.t.* injection). Data are mean ± SD, n = 3.

In addition to effectiveness, the safety of antitumor nanomedicines is also critical. The

biocompatibility of Pt/TCPP NCPs was revealed by bodyweight, histopathology, and serum biochemistry over time [6, 13]. As shown in Fig. S14A, the bodyweight of the mice escalated 20 days post-treatment with Pt/TCPP NCPs under 660 nm irradiation. Moreover, no obvious lesion was observed in the sections of the major organs (Fig. S14B). Besides, hepatorenal function assays (including AST, ALT, ALP, BUN, CREA, and LDH) also demonstrated that Pt/TCPP NCPs could efficiently avoid the hepatic and renal toxicity prevalent in a traditional cisplatin treatment (Fig. S14C). These results revealed the good systematic biocompatibility of Pt/TCPP NCPs *via i.t.* administration.

3. Supplementary Tables

Table S1. Measurement of molecular weight and composition of PE and PES polymers.

Abbreviation	Polymer	M_n [a], *k*Da		PDI [a]	MEO_2MA / OEGMA [b]		Sulfonate / EG [c]	
		M_n(Theo)	M_n(Meas)		*R*(Theo)	*R*(meas)	*R*(Theo)	*R*(meas)
PE	*p*(MEO_2MA_{120}-*co*-$OEGMA_{80}$)	47.0	47.3	1.08	1.50	1.50	/	/
PES	*p*(MEO_2MA_{120}-*co*-$OEGMA_{80}$)-*b*-*p*SS_{30}	53.2	54.1	1.09	1.50	1.50	0.15	0.15

[a]: M_n(Theo) was the theoretic value of number-average molecular weight (M_n), calculated from the feeding ratio between monomer and initiator. M_n(Meas) represented the measured values of M_n and polydispersity index (PDI), which were measured by GPC using 0.01 mol L^{-1} sodium nitrate solution as mobile phase and poly(ethylene glycol) (PEG) standards for calibration.

[b]: The molar ratio of MEO_2MA and OEGMA in PE. *R*(Theo) was the feeding ratio of the monomers, and *R*(Meas) was the measuring value of monomers amount in PE in terms of their ^1H NMR.

[c]: The molar ratio of sulfonate groups (SS) and ethylene glycol groups (EG, including MEO_2MA and OEGMA) in PES. *R*(Theo) was the feeding ratio of the monomers, and *R*(Meas) was the measuring value of monomers amount in PES in terms of their ^1H NMR.

Table S2. Hydrodynamic diameters and zeta potentials of Pt NCPs, TCPP NCPs and Pt/TCPP NCPs at the PES/TCPP ratio of 12.

	Hydrodynamic diameter (nm)	**Zeta potential (mV)**
Pt NCPs	269 ± 17.2	-16.3 ± 0.4
TCPP NCPs	160.2 ± 3.4	-22.9 ± 0.8
Pt/TCPP NCPs	144.9 ± 5.5	-14.3 ± 0.5

Table S3. Encapsulation efficiencies of TCPP and cisplatin in Pt/TCPP NCPs at various theoretical PES/TCPP ratios.

Theoretical PES/TCPP ratio	Encapsulation efficiencies of cisplatin (%)	Encapsulation efficiencies of TCPP (%)
0	99.76 ± 2.69	98.74 ± 1.16
3	98.68 ± 1.81	97.69 ± 2.52
6	99.08 ± 2.75	98.60 ± 1.90
12	96.14 ± 1.43	98.22 ± 1.29
18	97.28 ± 1.29	98.41 ± 1.81

Table S4. The theoretical and experimental ratios of PES/TCPP/cisplatin of Pt/TCPP NCPs at various theoretical PES/TCPP/cisplatin ratios according to their coordination ratios.

Theoretical PES/TCPP/cisplatin ratio	Experimental PES/TCPP/cisplatin ratio
0 : 1 : 1.00	0 : 1 : 1.01
2.97 : 1 : 3.98	3.01 : 1 : 4.02
5.94 : 1 : 6.94	6.01 : 1 : 6.97
11.88 : 1 : 12.89	12.08 : 1 : 12.62
17.83 : 1 : 18.82	18.10 : 1 : 18.61

Table S5. Drug loading capacity of Pt/TCPP NCPs at various theoretical PES/TCPP ratios.

Theoretical PES/TCPP ratio	cisplatin loading (%)		TCPP loading (%)	
	Theoretical	Measured	Theoretical	Measured
0	43.1	43.38 ± 1.17	56.9	56.62 ± 0.66
3	9.8	9.81 ± 0.18	3.3	3.22 ± 0.08
6	8.8	8.78 ± 0.24	1.7	1.66 ± 0.03
12	8.3	8.05 ± 0.12	0.9	0.84 ± 0.01
18	8.1	7.95 ± 0.11	0.6	0.56 ± 0.01

4. Supplementary References

1. W. J. Xu, X. L. Zhu, Z. P. Cheng, J. Y. Chen and J. M. Lu, *Macromol. Res.*, 2004, **12**, 32-37.
2. X. Li, X. L. Zhu, Z. P. Cheng, W. J. Xu and G. J. Chen, *J. Appl. Polym. Sci.*, 2004, **92**, 2189-2195.
3. J. S. Wan, S. N. Geng, H. Zhao, X. L. Peng, Q. Zhou, H. Li, M. He, Y. B. Zhao, X. L. Yang and H. B. Xu, *J. Control. Release*, 2016, **235**, 328-336.
4. M. Bonta, H. Lohninger, V. Laszlo, B. Hegedus and A. Limbeck, *J. Anal. Atom. Spectrom.*, 2014, **29**, 2159-2167.
5. M. Niemela, H. Kola, P. Peramaki, J. Piispanen and J. Poikolainen, *Microchim. Acta.*, 2005, **150**, 211-217.
6. H. Zhao, J. Xu, W. Huang, G. Zhan, Y. Zhao, H. Chen and X. Yang, *ACS Nano*, 2019, **13**, 6647-6661.
7. R. Kovacevic, M. Todorovic, D. Manojlovic and J. Mutic, *J. Iran. Chem. Soc.*, 2008, **5**, 336-341.
8. A. Soni, M. Chaudhary, V. K. Dwivedi, S. Kumar and S. M. Shrivastava, *Cardiovasc. Hematol. Disord. Drug Targets*, 2010, **10**, 138-142.
9. Y. Yingze, J. Zhihong, J. Tong, L. Yina, Z. Zhi, Z. Xu, X. Xiaoxing and G. Lijuan, *J. Neuroinflamm.*, 2022, **19**, 184.
10. S. Leary, W. Underwood, R. Anthony, S. Cartner, T. Grandin, C. Greenacre, S. Gwaltney-Brant, M. A. McCrackin, R. Meyer, D. Miller, J. Shearer, T. Turner and R. Yanong, *JAVMA-J. Am. Vet. Med. A.*, 2020, https://www.avma.org/resources-tools/avma-policies/avma-guidelines-euthanasia-animals.
11. S. C. Cartner, S. C. Barlow and T. J. Ness, *Comparative Med.*, 2007, **57**, 570-573.
12. X. F. Li, S. Khorsandi, Y. F. Wang, J. Santelli, K. Huntoon, N. Nguyen, M. M. Yang, D. Lee, Y. F. Lu, R. Q. Gao, B. Y. S. Kim, C. D. Lux, R. F. Mattrey, W. Jiang and J. Lux, *Nat. Nanotechnol.*, 2022, **17**, 891-899.
13. H. Zhao, J. Xu, C. Feng, J. Ren, L. Bao, Y. Zhao, W. Tao, Y. Zhao and X. Yang, *Adv. Mater.*, 2022, **34**, 2106390.
14. K. N. J. Burger, R. W. H. M. Staffhorst, H. C. de Vijlder, M. J. Velinova, P. H. Bomans, P. M. Frederik and B. de Kruijff, *Nat. Med.*, 2002, **8**, 81-84.
15. V. T. Huynh, J. Y. Quek, P. L. de Souza and M. H. Stenzel, *Biomacromolecules*, 2012, **13**, 1010-1023.
16. H. Zhao, Y. Zhao, J. Xu, X. Feng, G. Liu, Y. Zhao and X. Yang, *Chem. Eng. J.*, 2020, **398**, 125614.
17. R. W. Redmond and J. N. Gamlin, *Photochem. Photobiol.*, 1999, **70**, 391-475.
18. S. Y. Ye, J. M. Rao, S. H. Qiu, J. L. Zhao, H. He, Z. L. Yan, T. Yang, Y. B. Deng, H. T. Ke, H. Yang, Y. L. Zhao, Z. Q. Guo and H. B. Chen, *Adv. Mater.*, 2018, **30**, 1801216.
19. Z. Y. Hu, Y. F. Pan, J. W. Wang, J. J. Chen, J. Li and L. F. Ren, *Biomed. Pharmacother.*, 2009, **63**, 155-164.
20. G. C. Yu, T. R. Cook, Y. Li, X. Z. Yan, D. Wu, L. Shao, J. Shen, G. P. Tang, F. H. Huang, X. Y. Chen and P. J. Stang, *Proc. Nat. Acad. Sci. U.S.A.*, 2016, **113**, 13720-13725.
21. J. Y. Zeng, M. Z. Zou, M. K. Zhang, X. S. Wang, X. Zeng, H. J. Cong and X. Z. Zhang, *ACS Nano*, 2018, **12**, 4630-4640.
22. K. N. Zhu, S. Y. Qian, H. W. Guo, Q. Y. Wang, X. Y. Chu, X. Y. Wang, S. Lu, Y. Peng, Y. S. Guo, Z. Q. Zhu, T. Y. Qin, B. Liu, Y. W. Yang and B. L. Wang, *ACS Nano*, 2022, **16**, 11136-11151.
23. Z. Q. Guo, H. He, Y. Zhang, J. M. Rao, T. Yang, T. Li, L. Wang, M. K. Shi, M. Y. Wang, S. H. Qiu, X. Song, H. T. Ke and H. B. Chen, *Adv. Mater.*, 2021, **33**, 2004225.
24. M. T. Oztek, M. D. Hampton, D. K. Slattery and S. Loucks, *Int. J. Hydrogen Energy*,

2011, **36**, 6705-6710.
25. S. C. Doan, S. Shanmugham, D. E. Aston and J. L. McHale, *J. Am. Chem. Soc.*, 2005, **127**, 5885-5892.
26. Q. L. Zou, M. Abbas, L. Y. Zhao, S. K. Li, G. Z. Shen and X. H. Yan, *J. Am. Chem. Soc.*, 2017, **139**, 1921-1927.
27. N. Tsapis, D. Bennett, B. Jackson, D. A. Weitz and D. A. Edwards, *Proc. Nat. Acad. Sci. U.S.A.*, 2002, **99**, 12001-12005.
28. Z. Q. Guo, Y. L. Zou, H. He, J. M. Rao, S. S. Ji, X. N. Cui, H. T. Ke, Y. B. Deng, H. Yang, C. Y. Chen, Y. L. Zhao and H. B. Chen, *Adv. Mater.*, 2016, **28**, 10155-10164.
29. H. He, S. S. Ji, Y. He, A. J. Zhu, Y. L. Zou, Y. B. Deng, H. T. Ke, H. Yang, Y. L. Zhao, Z. Q. Guo and H. B. Chen, *Adv. Mater.*, 2017, **29**, 1606690.
30. T. Yang, L. Liu, Y. B. Deng, Z. Q. Guo, G. B. Zhang, Z. S. Ge, H. T. Ke and H. B. Chen, *Adv. Mater.*, 2017, **29**, 1700487.